Numerical Simulation and Validation of Motor Dynamics in Reciprocating Compressor Driveline Coupled with Stiff and Soft Elastic Couplings under Continuous and Transient Operating Conditions

Dr. M. Hasan
Global Simulation Manager
REXNORD CENTA
Bergische Strasse 7, 42781 Haan/Germany

M. Naumann
R&D Engineer
NEUMAN & ESSER GmbH & Co. KG
52531 Übach-Palenberg, Germany

Dr. Mahamudul Hasan is working at REXNORD CENTA as a Global Simulation Manager for the sector energy under PMC platform. He is experienced in numerical simulation in the field of physical vibration dynamics and finite element modelling in drivetrain technology. He has made his PhD in Mechanical Engineering and M.Sc in Computational Engineering from Ruhr University of Bochum, Germany.

Marcel Naumann is R&D engineer at Neuman & Esser GmbH & Co. KG – Central Division of Technology since 2006. He has experience in compressor design, torsional analysis, pulsation studies, FEA and fatigue analysis. He has made his Dipl.-Ing. (FH) for mechanical engineering at the University of Applied Sciences in Cologne.

ABSTRACT

Reciprocating compressor is often used in the field of gas compression industry and generates harmonic torque excitation in a driveline. The objective of this paper is to simulate the dynamic torsional vibrations by considering motor as an electromechanical system with real electrical characteristics and solve them numerically in order to capture the accurate torque oscillations inside couplings. The wrong selection of coupling may lead to the damage of the coupling as well as the components connected in the driveline as they produce high level of vibrations. A large deviation of torque fluctuations has been observed with two different approaches between simple model as spring damper and multiphysics motor model. The accuracy can be achieved with a user defined electromechanical motor model and the negative damping effect is accomplished without tuning the model. Finally, the simulation results were compared with measured experimental data. The validation shows a good match. The final models are based on validation concept. Two examples are presented with flexible and torsional stiff couplings in order to optimize the coupling for a higher system reliability in a particular driveline. The flexible coupling shows relatively low vibratory torque in the coupling compared to torsional stiff coupling. The damping and dynamic stiffness of rubber couplings play an important role to attenuate vibration as the coupling mode shape controls the vibration signature. Moreover, the transient loading under short circuit event and energy saving valve unloaders operating conditions haven been investigated that are used in many reciprocating compressors applications.

Introduction

The reciprocating machines produce dynamic loads due to their crank mechanisms. The dynamic torque excitation of a reciprocating compressor needs to be considered during torsional vibration analysis. Soft elastic rubber or steel disc couplings are used to transmit torque and reduce torsional vibrations in drivelines, effectively isolating the prime mover from the driven equipment. The excitation torque variations along the crank angle provide the signature of vibration and it has a profound influence on the vibratory amplitudes. It is extremely important to capture the amount of allowable vibratory torque in the elastic coupling for a suitable selection. The motivation of this paper is to develop a complete driveline model including electro-mechanical properties [1-3] to characterize the vibration of coupled reciprocating compressor as the dynamic torque fluctuations influence the magnitude of vibration. It helps to select the optimized coupling for a particular application for a higher system reliability.

Reciprocating compressors produce considerable torque variations along the crank angle that results in torsional excitation into the drivetrain [4-6]. If the rotor has a torsional velocity fluctuation, it will superimpose over the constant steady rotation. Under this condition, the flux linkages oscillate from electrical motor. This phenomenon influences the electromagnetic fields across the air gap between stator and rotor. It generates an additional torque with rotor harmonic excitation.

Model development of coupled electrical motor

The electrical behavior [7-10] of induction motor plays an important role in torsional vibration analysis, and it is necessary to simulate its contribution. In this work, a multi-physics approach has been utilized. Figure 1 shows the schematic diagram of electromechanical model concept and it is obvious that differential equations of the non-linear system composed by both electrical and mechanical part, which represent the induction motor as well as coupled driveline with soft coupling. The electrical behavior of induction motor is modelled by using following differential equation.

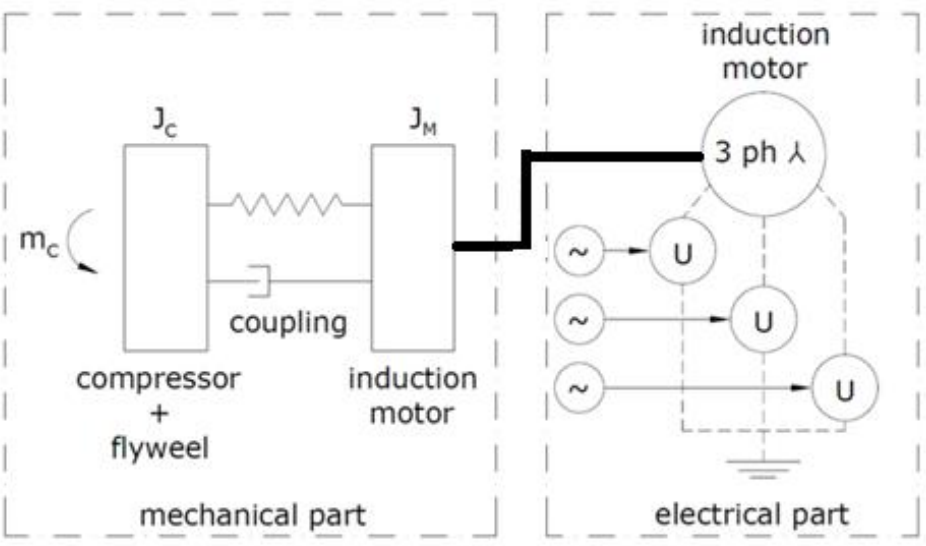

Figure 1: Schematic presentation of electromechanical model concept

Voltage and magnetic flux equations are formulated below:

$$u_1 = i_1 R_1 + \frac{d\Psi_1}{dt} \qquad \text{(Eq. 1)}$$

$$0 = i_2 R_2 + \frac{d\Psi_2}{dt}$$

$$\Psi_1 = i_1 L_1 + i_2 L_h e^{jp\beta}$$

$$\Psi_2 = i_2 L_2 + i_1 L_h e^{-jp\beta}$$

The motor air gap torque formulated as a conjugated complex form as shown in Eq.2.

$$m_M = \frac{3}{2} p.\ I_m\ \{\Psi_2\ .\ i_2^*\} \qquad \text{(Eq. 2)}$$

R = ohm's resistance,
L = inductivity
Ψ = magnetic flux
u = voltage
i= current
β = angle between rotor and stator coil
p= number of pole pairs
Index 1 = stator, index 2 = rotor
m_M = motor air gap torque
j = imaginary number
I_m = imaginary part
*= conjugated complex
ω= angular frequency of the given harmonic
m_C = compressor torque

The multi-mass model differential equation is formulated as below which includes the compressor excitation and motor air gap torque. Please note that the model incorporates the electrical behavior

$$J_N \frac{d^2\theta(t)}{d^2t} + K_N\theta(t) + D_N \frac{d\theta(t)}{dt} = T_{ext} \qquad \text{(Eq. 3)}$$

$$T_{ext} = m_M + m_C$$

The mechanical system is described as a matrix equation. The mass moment of inertia J, the damping D and the stiffness K can be varied from 1 to N. Particular attention was paid to model the induction motor with electrical differential equations and couple them into mechanical domain [4-6].

Driveline description

A diagram of the motor–driven compressor train is shown in Figure 2. The induction motor is rated at 230 kW. The two-stage reciprocating compressor has a speed of 425 RPM.

Figure 2: Schematic diagram of motor-driven Compressor drivetrain coupled with soft elastic coupling

Operating conditions

The following operating conditions are modelled:

1. 100% capacity operating condition (steady state)
2. 50% capacity valve unloaders operating condition (steady state)
3. 2-phase short circuit (transient)
4. 3-phase short circuit (transient)

Steady state load cases

The steady state operating condition is often used to select a suitable coupling and also justify the loading on motor shaft as well as other connected structural parts. This paper also documents the transient operating condition with two examples for two and three phase short circuit events to investigate the loading on coupling and motor shaft. In addition, valve unloaders are used to control the effective capacity and also for energy savings in many reciprocating compressors. A common solution is for a cylinder to run at half load (Figure 3).

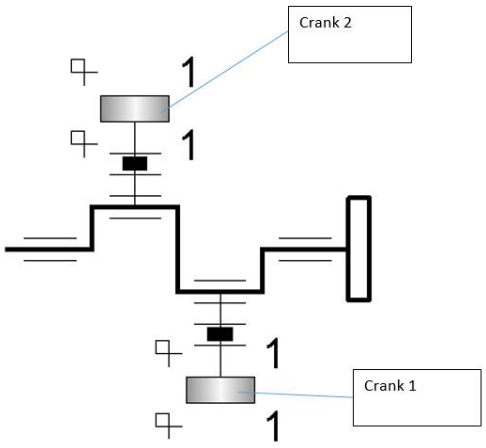

a) Both double acting cylinders are working at 100% capacity (filled white symbols indicate valves are not lifted)

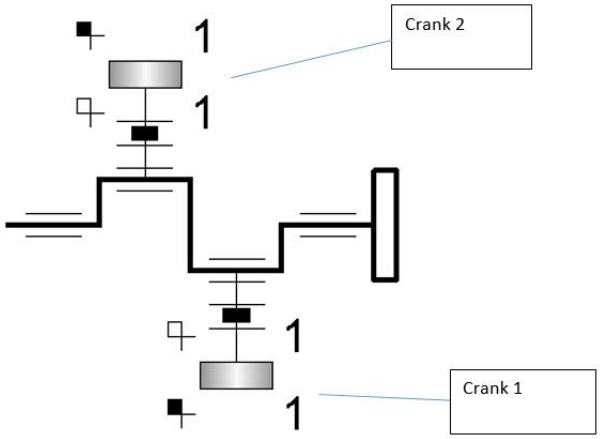

b) The head end suction valves are lifted (filled black symbols). Compressor is running at 50% capacity.

Figure 3: Schematic presentation of compressor with horizontal 2 crank machines are equipped with a suction valve unloader [13]

Transient load cases

Drivetrains are designed to withstand not avoidable high transient loads such as 2- and 3- phase short circuit events. A lightning strike into the overhead line can lead to a 2- or 3- phase short circuit.

2-phase short circuit

The 2-phase short circuit event can be observed when two feed lines are shorted. The 2-phase short circuit leads to a shock torque with 1st and 2nd order harmonics of the grid frequency. The height of the excitation is dependent on initial time point [12]. Therefore, it is important to vary time points with a tolerance from initial condition to investigate the worst-case loading.

3-phase short circuit

The 3-phase short circuit event can be observed when three feed lines are shorted. The 3-phase short circuit leads to a shock torque with 1st order harmonic of the grid frequency. The height of the motor excitation is independent of initial time point due to its symmetrical loading [12]. There is a minor influence of the mechanical initial time point and it can be neglected.

Results and Discussions

Time-domain response calculations are performed using the proprietary simulation tool KO3, developed by Neuman & Esser [13]. The time domain simulation is conducted on driveline model and validate with measured data. The drive train model consists of a reciprocating compressor, flywheel, steel disc coupling and asynchronous motor (1000kW, 496RPM). The compressor 1+1SZL300 is a horizontal 2 crank machine with 2 processes and is equipped with a suction valve unloader. The mass-elastic data of this driveline can be found in Table 1. Fig. 4 provides the comparison between simulation and measurements. The strain gauge measurement was applied on the coupling spacer. The blue and red curves represent the simulated and measured data respectively. A very good match has been obtained with only 2% deviation. Furthermore, the validated model concept is used for further vibration analysis with all models.

i	**Name**	**J_i [kgm^2]**
1	Cranks	15.5
2	Flywheel	890
3	Coupling	14.9
4	ASyn Motor	289

i	**Name**	**c_i [MNm/rad]**
1	Crankshaft	14.9
2	Coupling	7.4
3	Motorshaft	13

Table 1: Mass moment of inertia and stiffness data for driveline for the validation model

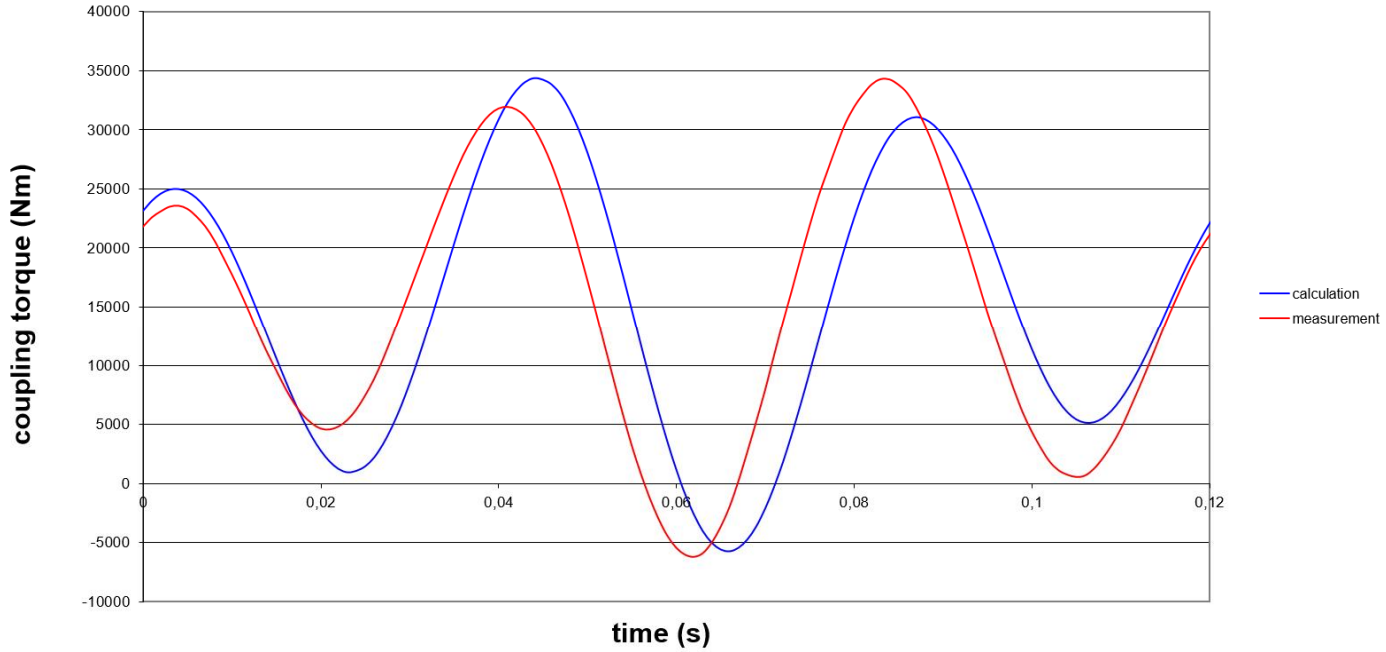

Figure 4: Calculated (blue) and measured (red) coupling vibratory torque

For our further analysis, Two different models are used and the descriptions can be found below:

Mass moment of inertia

i	Name	J_i [kgm²]
1	Crank 2	0.93
2	Crank 1	0.93
3	Flywheel+Coupling 1	159
4	Coupling 2	0.9
5	ASyn Motor	159

Torsional stiffness

i	Name	c_i [MNm/rad]
1	Crankshaft 2	6.29
2	Crankshaft 1	2.30
3	Coupling_c	0.047
4	Motorshaft	6.22

Table 2: Mass moment of inertia and stiffness data for driveline with elastic (soft coupling) [13]

i	Name	J_i [kgm²]
1	Crank 2	0.93
2	Crank 1	0.93
3	Flywheel+Coupling 1	159
4	Coupling 2	0.16
5	ASyn Motor	159

Torsional stiffness

i	Name	c_i [MNm/rad]
1	Crankshaft 2	6.29
2	Crankshaft 1	2.50
3	Coupling_c	2.14
4	Motorshaft	6.22

Table 3: Mass moment of inertia and stiffness data for driveline with all steel disc coupling (rigid coupling) [13]

From Table 2 & 3, it is obvious that the elastic coupling is 45 times softer than stiff coupling and it has a remarkable influence on the

first natural frequency. Table 4 & 5 documented the mode shapes and natural frequencies for the complete driveline. The first mechanical TNF is occurred at 3.83 Hz with elastic coupling and 22.4 Hz with torsionally stiff coupling.

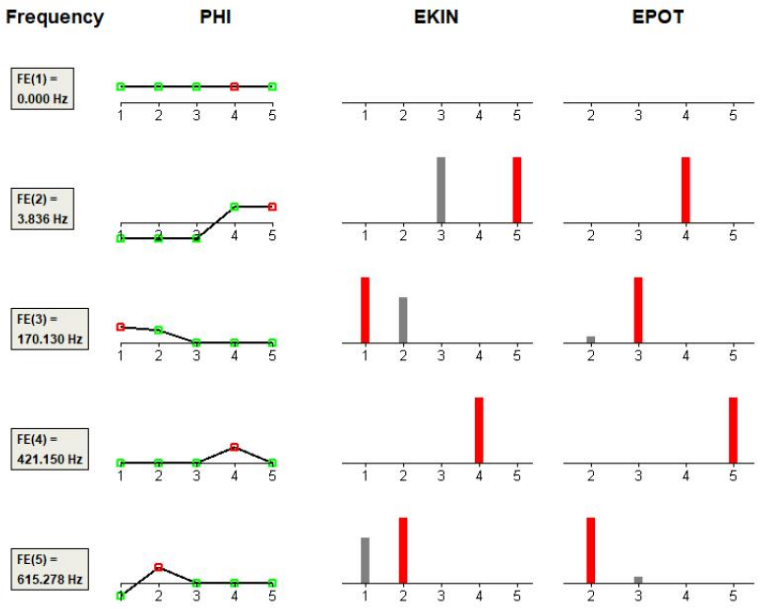

Table 4: Mode shapes and natural frequencies for torsional system with elastic (soft) rubber coupling [13]

It depicts the fact that the biggest deflection occurs inside the couplings as their dynamic stiffnesses are softer than other connected structural stiffnesses. This is a big advantage of the highly flexible rubber coupling because all possible deviations of the motor shaft stiffness have no effect [3]. During operation, this mechanical natural frequency is shifted to a higher value because of the influence of the motor magnetic field [1]. The electro-mechanical natural frequency is always somewhat higher than the mechanical natural frequency. The motor always influences the mechanical natural frequency, when the rotor vibrates in magnetic field. Checking the rotor kinetic energy (EKIN) at mode shape calculation helps to identify if a natural frequency can be influenced by the magnetic field.

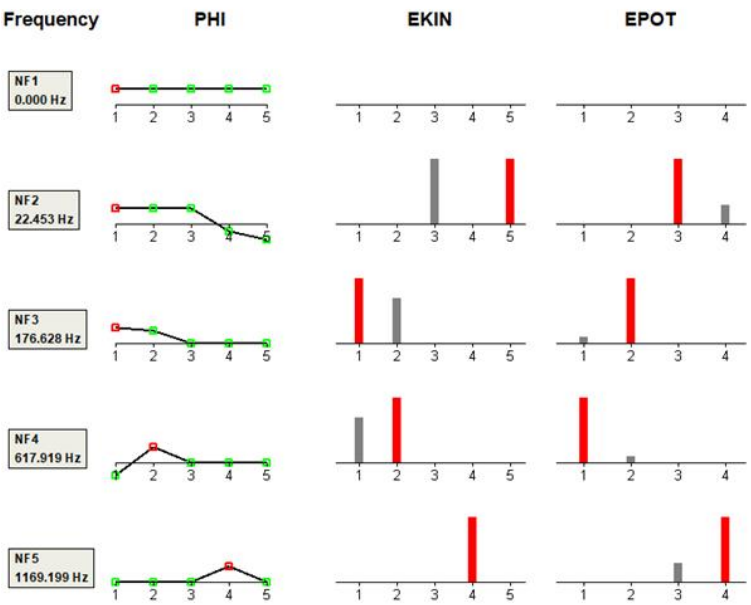

Table 5: Mode shapes and natural frequencies for torsional system with all steel disc coupling [13]

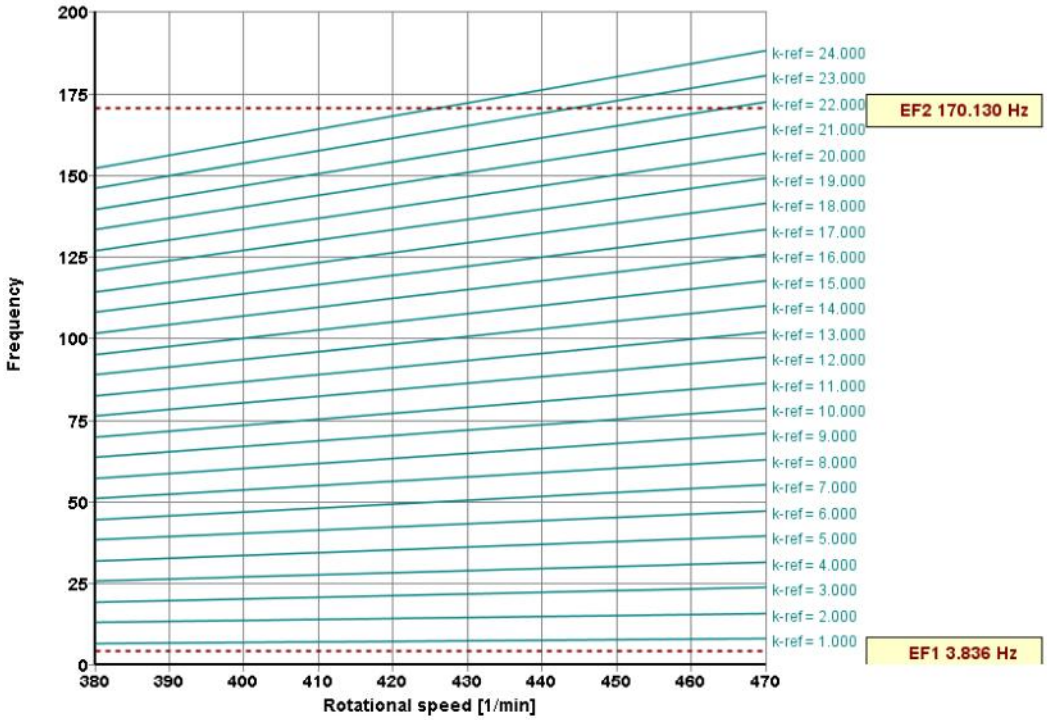

Figure 5: Campbell diagram represents torsional natural frequencies over rotational speed for torsionally soft coupling [13]

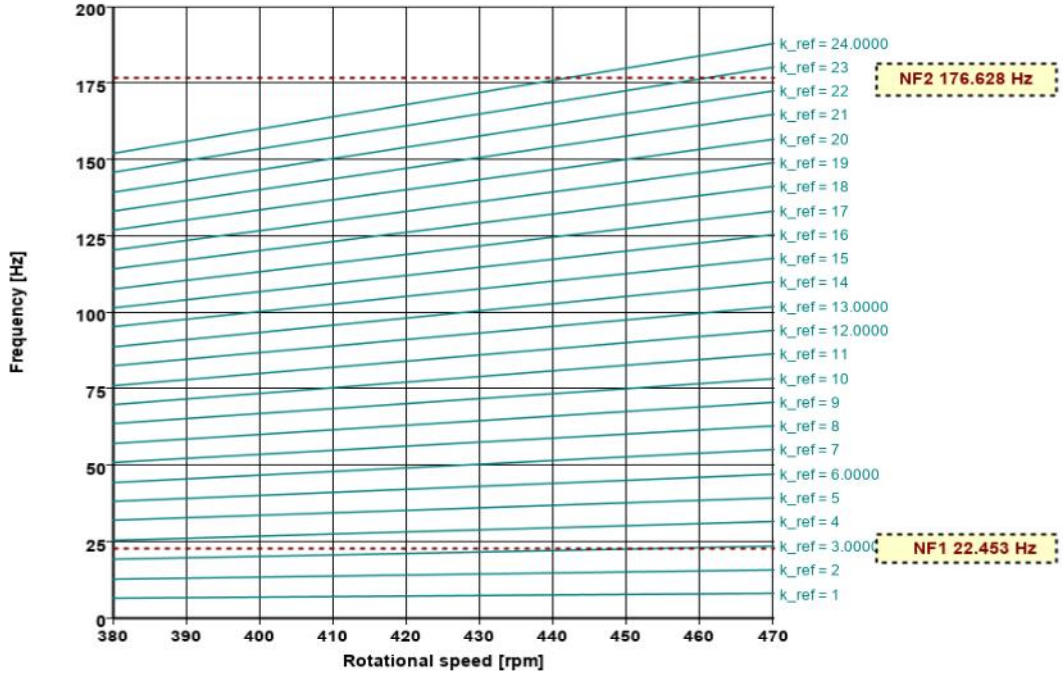

Figure 6: Campbell diagram represents torsional natural frequencies over rotational speed for torsionally stiff coupling [13]

The campbell diagrams are shown in Figures 5 & 6. It is noticeable that the mechanical natural frequency in case of soft elastic coupling has a good separation margin from excitation frequency of 7 Hz. In case of torsionally stiff coupled driveline the 3rd harmonic order provides an interference with 22 Hz.

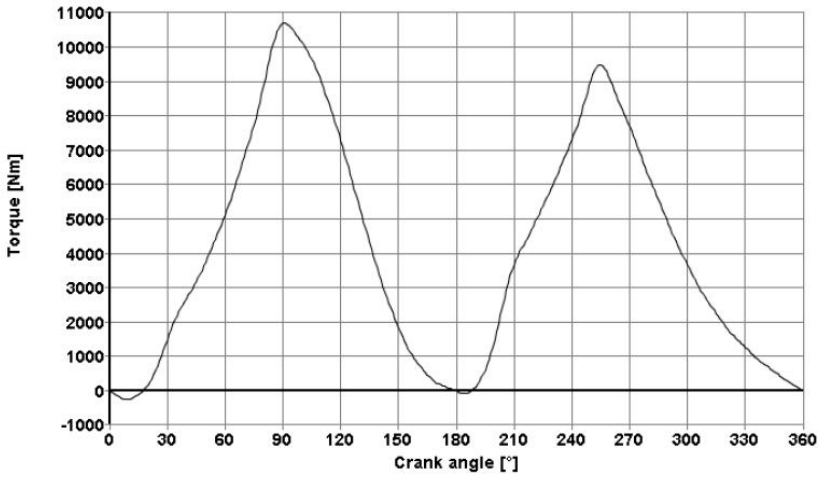

Figure 7: compressor torque variation as a function of crank angle for one complete revolution of the crankshaft for 100% load [13]

In order to analyze the resulting torsional vibration, the spectrum of the dynamic components of the torque is generated as shown in Figures 7-10.

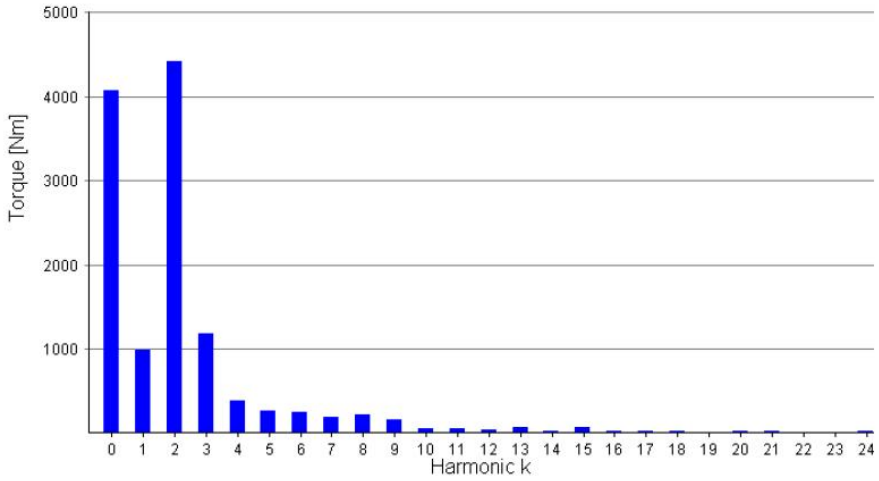

Figure 8: Spectrum of excitation torque for 100% load [13]

From Figures 7 & 9, it is obvious that the compressor torque variation as a function of crank angle are altering as the amount of load changes. In case of half load of cylinder, 1st order harmonic torque magnitude is increased compared to 100 % load (Figure 8 & Figure 10). Please note that 0th harmonic order presents the mean torque of motor. The load dependent motor excitation torque, vibratory torque in the soft coupling and the motor shaft vibratory torque is shown in Figures 11-13 & Figures 15-17. A higher magnitude of vibratory torque has been observed in the soft coupling for 50% load compared to 100% load. Results were compared by the coupling manufacturer with the allowable limits for vibratory torque and they are below allowable limit.

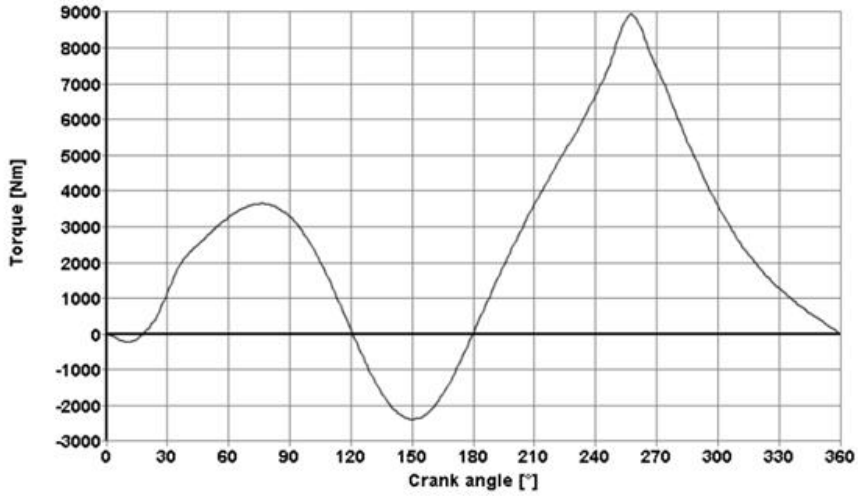

Figure 9: compressor torque variation as a function of crank angle for one complete revolution of the crankshaft for 50% load [13]

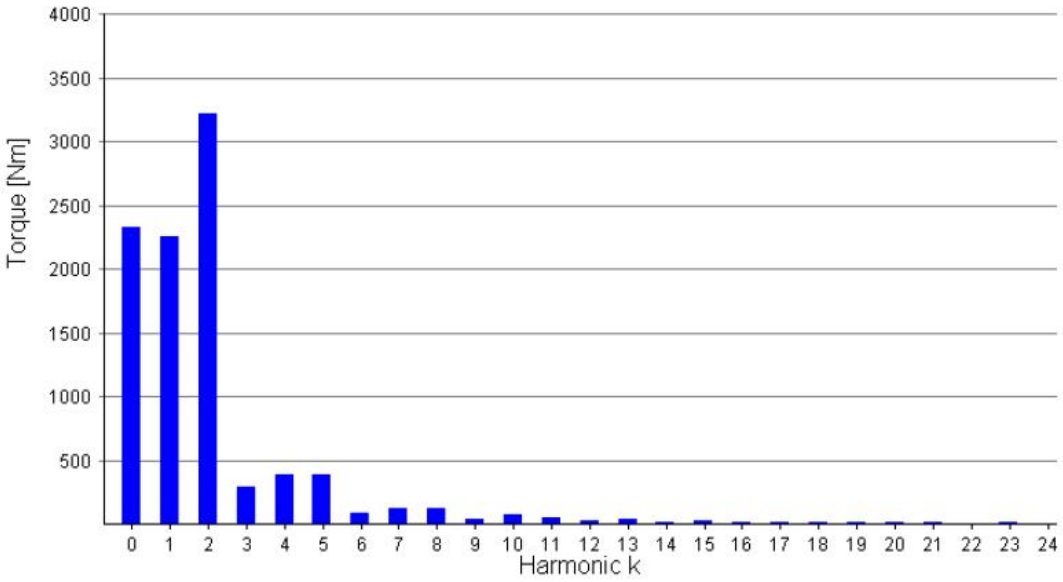

Figure 10: Spectrum of excitation torque for 50% load [13]

The results of the time domain simulations can be found in the appendix (Figures 11-39).
From Figures 14, 18, 28 and 32, it is noticeable that the current variation limit acc. API 618 (5th edition) paragraph 7.1.2.6 of 40% is not exceeded. The current pulsations are a result of the calculation and can be compared to the current pulsation limits according to API 618 [11]. This is a big advantage of a numerical simulation including the mechanical- and electrical- part of a drivetrain.

The transient operating condition results under short circuit event are shown in Figures 19-23. It can be visualized that the asynchron motor excitation torque of 2-phase short circuit is different compared to the 3-phase short circuit. The higher amount of vibratory torque in case of 3-phase short circuit is being noticed. Nevertheless, it is below the allowable limit.

It is interesting to observe from Figures 25 & 29 that the motor excitation torque pattern varies with loads. The soft coupling vibratory torque and motor shaft torque have a lower magnitude compared to stiff/rigid coupling (Figures 12,13,16,17,26,27,30,31). Please note that the 3rd harmonic order is at 21.25 Hz and it has conflict with stiff coupled natural frequency in this driveline. The 3rd harmonic response has been observed with stiff coupling in time domain calculation.

It is also evident that the soft coupling provides better level of torque under short circuit event (Figures 19-24 & Figures 33-38).

The sweep functions (Figure 39) are obtained by varying the dynamic stiffness of coupling in 51 increments. This is done to include modeling uncertainties within the stiffness values. For each increment, a time domain simulation is performed, and the maximum and minimum coupling torque load is plotted. A peak can be found at sweep index 17 in case of stiff coupling whereas there is no evidence of peak in elastic coupling. It is a pretty common that the highly flexible coupling shows no resonance peak even if it is running in resonance, when the driver is an asynchronous motor. Drivetrain with steel disc coupling cannot avoid the resonances because of coupling stiffness uncertainties. The first mode resonance is occurring at a higher frequency (2nd – 5th harmonic) and the motor is not able to reduce the torque loads.

Conclusions

The work reports the numerical modelling of induction motor in a physical domain. The compressor torque varies along the crank angle and it has an influence on rotor torque. Torsionally soft coupling provides better operational reliability compared to all steel disc coupling. Motor shaft stress values are less with soft couplings compared to stiff couplings. The dynamic stiffness of rubber couplings play an important role as the coupling mode shape controls the vibration pattern. The induction motor has longer time to control the vibration with elastic soft coupling as the natural frequency is very low compared to stiff coupling. Torsionally soft couplings also provide less vibratory torque under transient event, because the natural frequency is far away from the excitation frequencies.

References

[1] Knop, G., “The Importance of Motor Dynamics in Reciprocating Compressor Drives,” EFRC, Dösseldorf (2012).

[2] Knop, G., “Entwicklungsschritte bei der drehschwingungsgerechten Auslegung von Antriebssträngen mit Kolbenverdichtern, 5. Kötter Workshop Kolbenverdichter“, 2001

[3] Knop, G., Dr. Hoff, K., „Pros and Cons of Various Coupling Types for Reciprocating Compressor Installations“, EFRC, Prague (2007)

[4] Feese, T.D., and Hill, C.H., “Guidelines for Preventing Torsional Vibration Problems in Reciprocating Machinery”, Gas Machinery Conference, Nashville, Tennessee (2002).

[5] Wang, Q., Feese, T. D., and Pettinato, B. C., “Torsional Natural Frequencies: Measurement vs. Prediction”, Proceedings of the 41st Turbomachinery Symposium, Turbomachinery Laboratory, Texas A&M University, College Station, Texas (2012).

[6] Feese, T., "Coupling failure in engine-driven pipeline compressor system", TVS 2017

[7] Kocur, J.A. and Muench, M.G., “Impact of Electrical Noise on the Torsional Response of VFD Compressor Trains,” Proceedings of the First Middle East Turbomachinery Symposium (2011)

[8] Jordan, H., Muller, J., Seinsch, H.O., “Über Das Verhalten von Drehstromasynchronmotoren in drehelastischen Antrieben”, AEG-Telefunken (1980).

[9] Hauptmann, E.G., Eckert W.F., Howes B.C., “The Influence on Torsional Vibration Analysis of Electromagnetic Effects Across

an Induction Motor Air-gap", Gas Machinery Conf. (2013).
[10] Adachi, A., Murphy, B., "Torsional Instability of Cooling Tower Fan during Induction Motor start-up", 45th Turbomachinery & 32nd Pump Symposia, Houston (2016).
[11] API Standard 618, "Reciprocating Compressors for Petroleum, Chemical, and Gas Industry Services," American Petroleum Institute, www.api.org, Washington D.C.
[12] Seinsch, H.O., "Ausgleichsvorgänge bei elektrischen Antrieben: Grundlagen zur analytischen und numerischen Berechnung", B.G. Teubner Stuttgart, 1991
[13] Neuman & Esser, proprietary compressor design tool KO³

Appendix

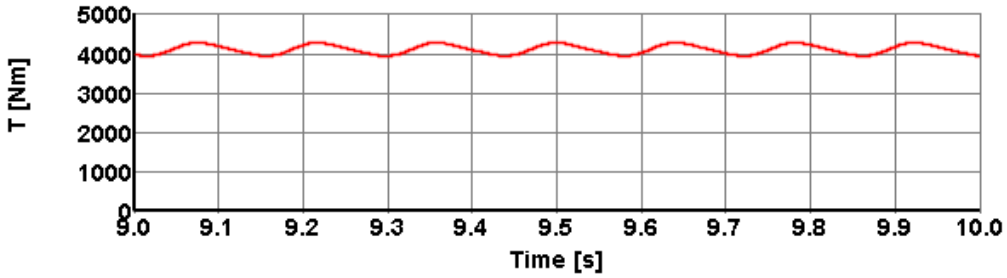

Figure 11: excitation torque of induction motor coupled with soft coupling for 100 % load [13]

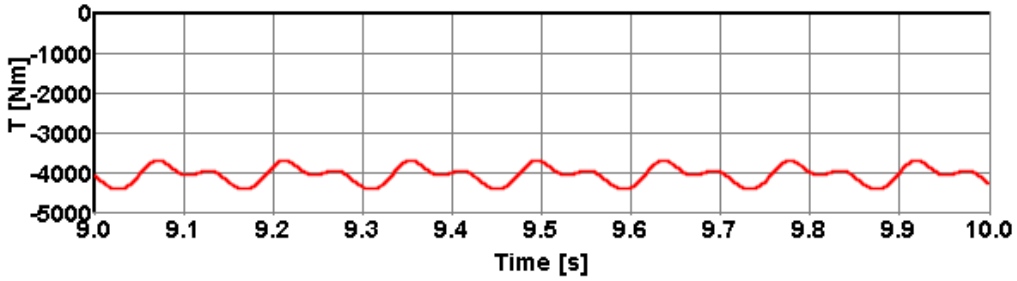

Figure 12: Vibratory torque in elastic/soft coupling for 100% load [13]

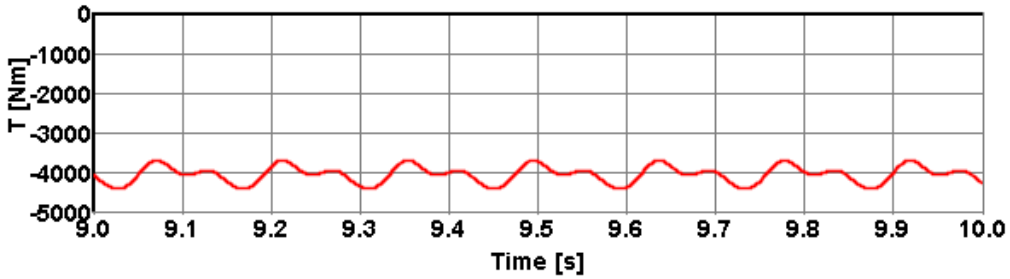

Figure 13: Vibratory torque in motor shaft for 100% load [13]

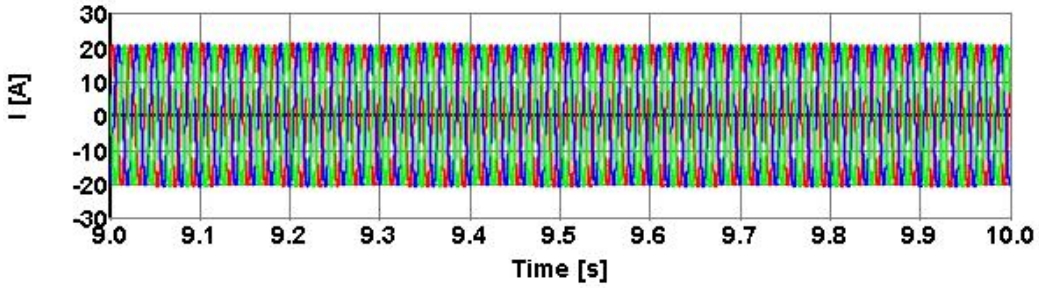

Figure 14: Stator current in asynchron motor for 100% load [13]

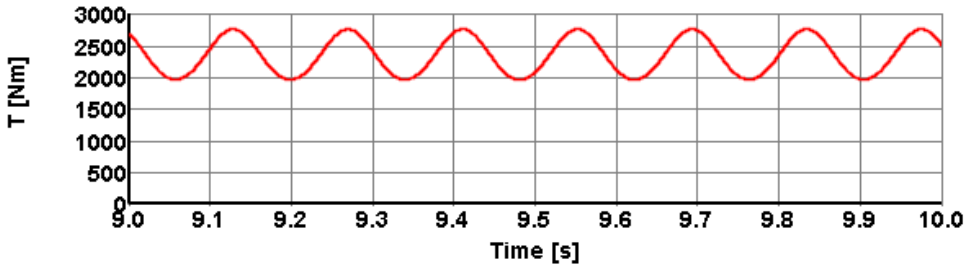

Figure 15: excitation torque of induction motor coupled with soft coupling for 50 % load [13]

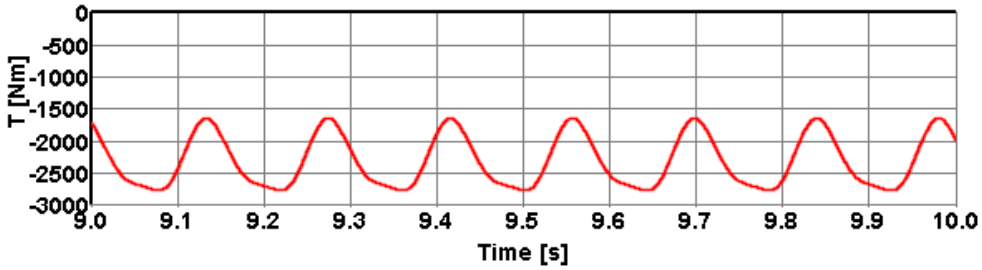

Figure 16: Vibratory torque in elastic/soft coupling for 50% load [13]

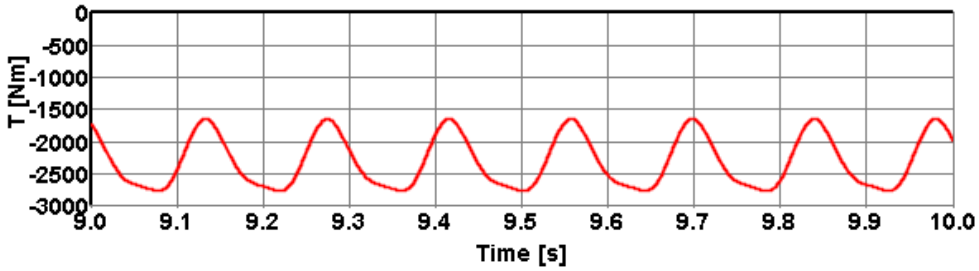

Figure 17: Vibratory torque in motor shaft for 50% load [13]

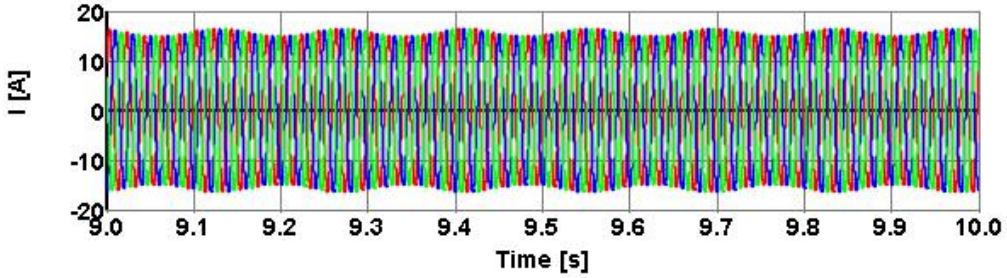

Figure 18: Stator current in asynchron motor for 50% load [13]

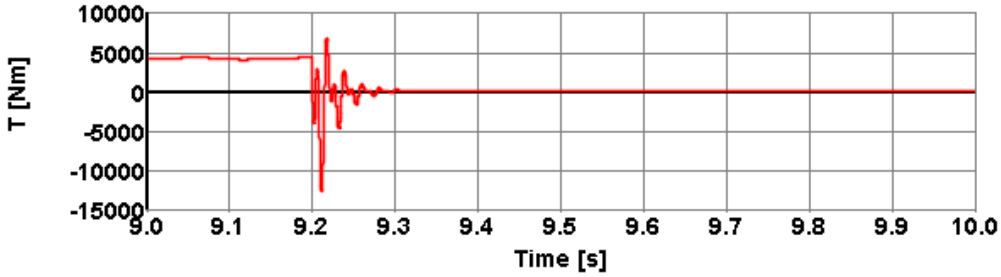

Figure 19: Excitation torque of asynchron motor under 2-phase short circuit event [13]

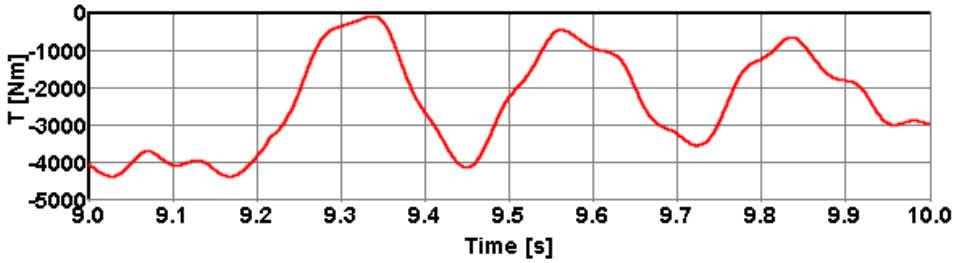

Figure 20: Vibratory torque in elastic/soft coupling under 2-phase short circuit event [13]

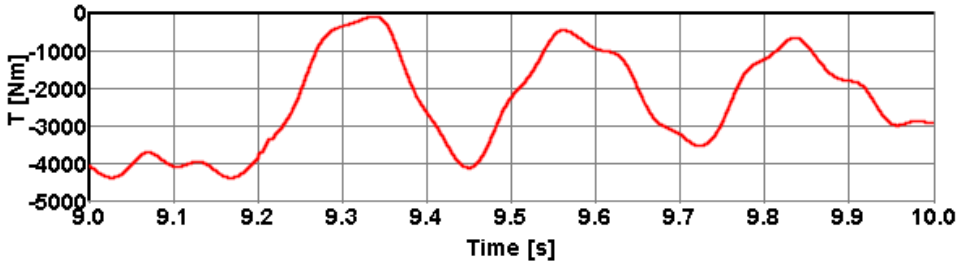

Figure 21: Vibratory torque in motor shaft with soft coupling under 2 phase short circuit event [13]

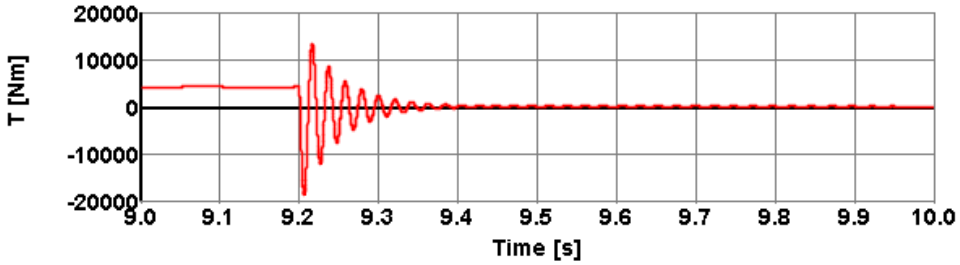

Figure 22: Excitation torque of asynchron motor under 3-phase short circuit event [13]

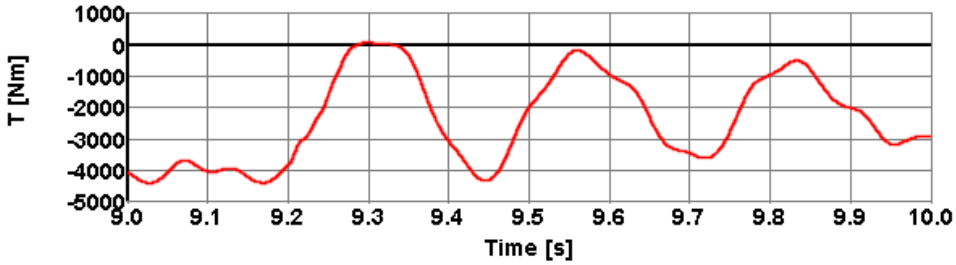

Figure 23: Vibratory torque in elastic/soft coupling under 3-phase short circuit event [13]

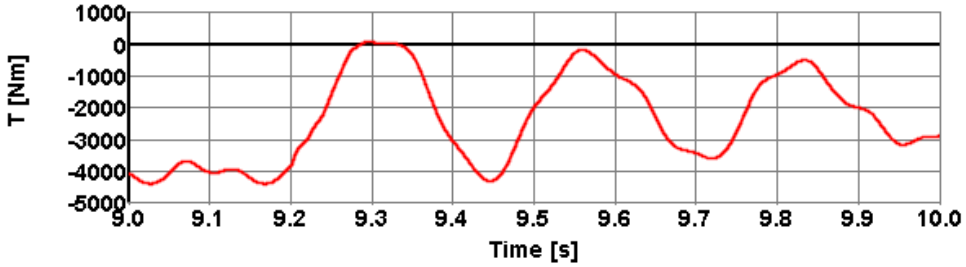

Figure 24: Vibratory torque in motor shaft with soft coupling under 3-phase short circuit event [13]

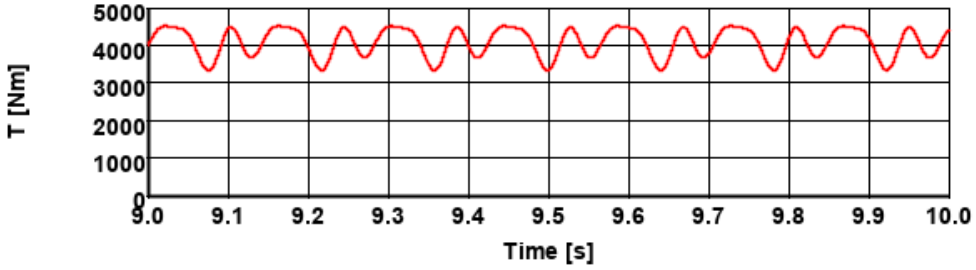

Figure 25: excitation torque of induction motor coupled with stiff/rigid coupling for 100 % load [13]

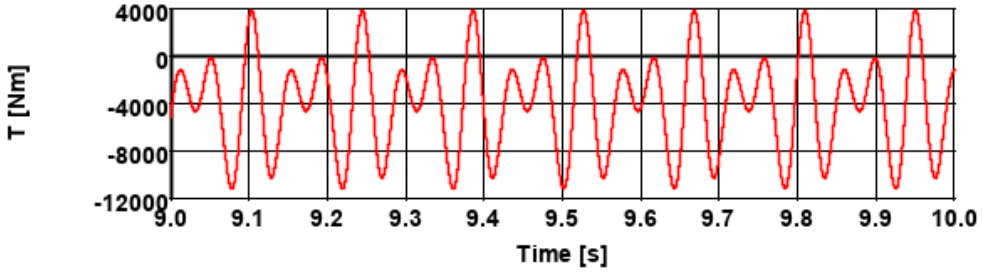

Figure 26: Vibratory torque in stiff/rigid coupling for 100% load [13]

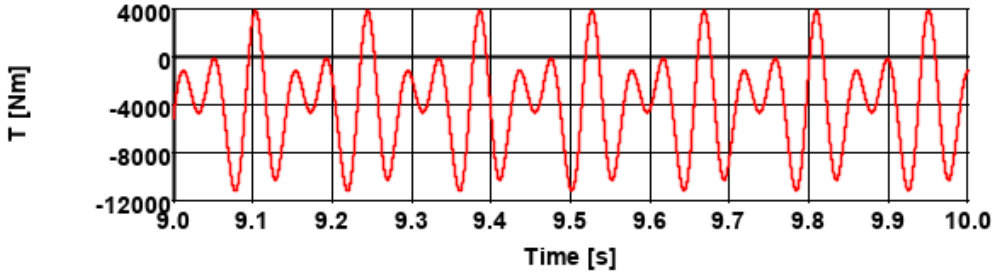

Figure 27: Vibratory torque in motor shaft for 100% load with stiff coupling [13]

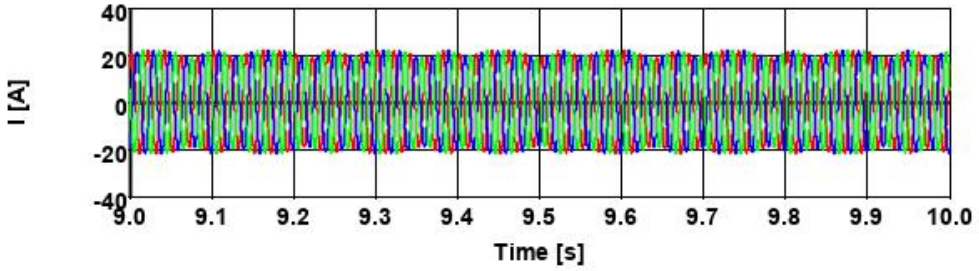

Figure 28: Stator current in asynchron motor for 100% load with stiff coupling [13]

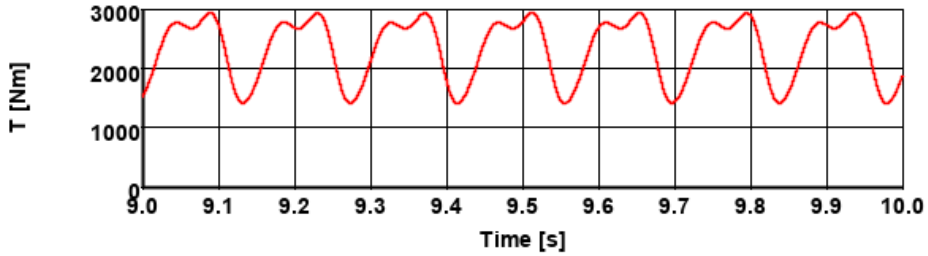

Figure 29: excitation torque of induction motor coupled with stiff/rigid coupling for 50 % load [13]

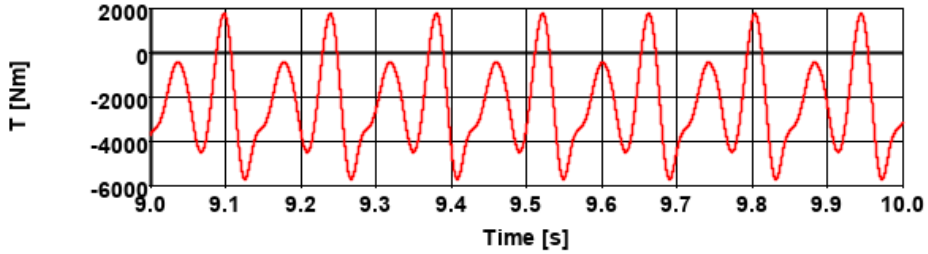

Figure 30: Vibratory torque in Stiff/rigid coupling for 50% load [13]

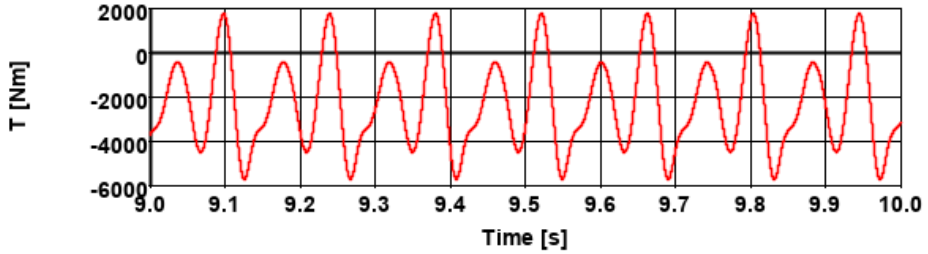

Figure 31: Vibratory torque in motor shaft for 50% load with stiff coupling [13]

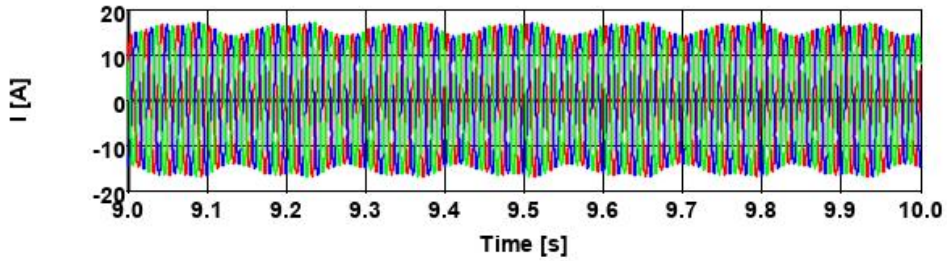

Figure 32: Stator current in induction motor for 50% load with stiff coupling [13]

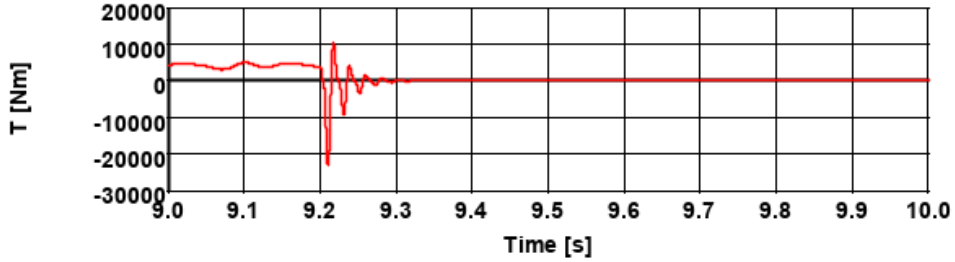

Figure 33: Excitation torque of asynchron motor under 2-phase short circuit event with stiff coupling [13]

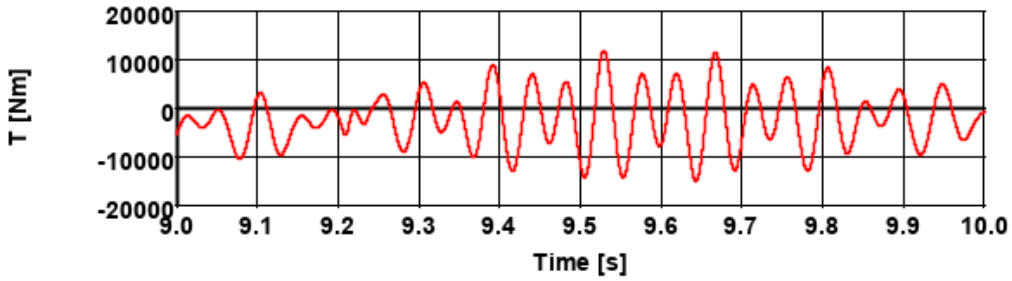

Figure 34: Vibratory torque in stiff coupling under 2-phase short circuit event [13]

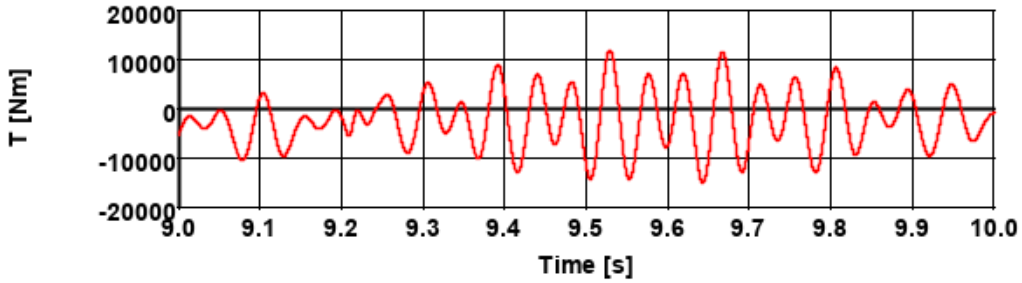

Figure 35: Vibratory torque in motor shaft under 2 phase short circuit event with stiff coupling [13]

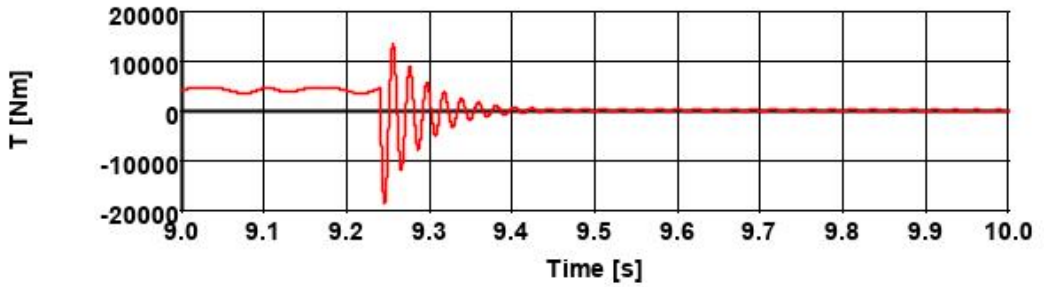

Figure 36: Excitation torque of asynchron motor under 3-phase short circuit event with stiff coupling [13]

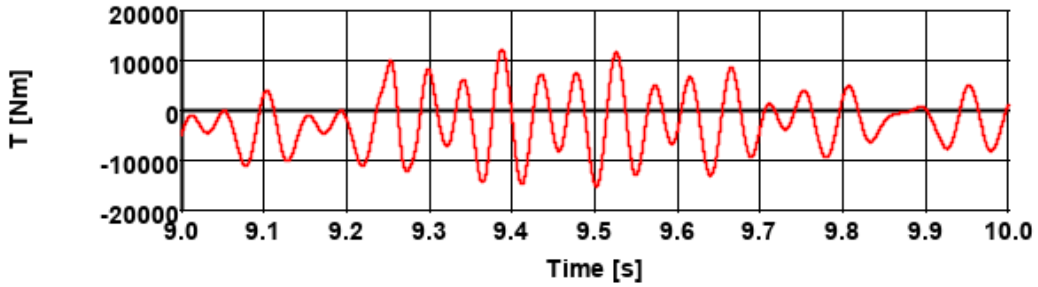

Figure 37: Vibratory torque in stiff coupling under 3-phase short circuit event [13]

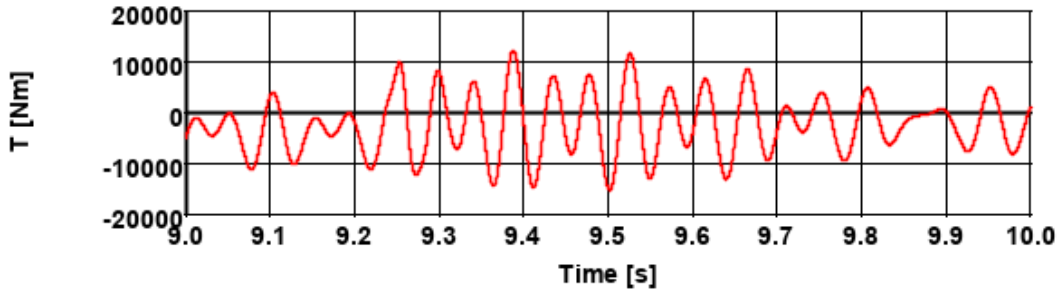

Figure 38: Vibratory torque in motor shaft under 3 phase short circuit event with stiff coupling [13]

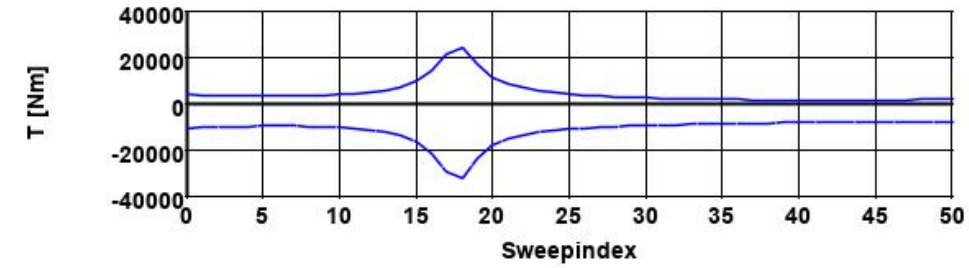

a)

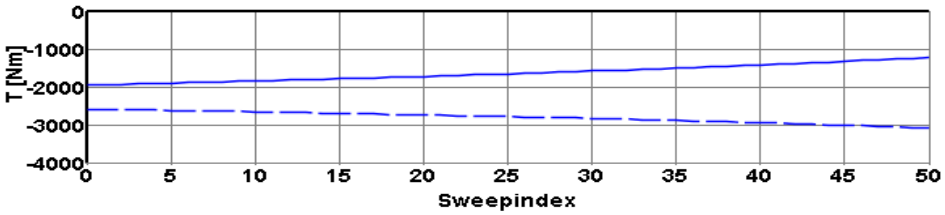

b)

Figure 39: Visualization of sweep functions a) Torsionally stiff b) Torsionally soft couplings [13]